JACS
JOURNAL OF THE AMERICAN CHEMICAL SOCIETY
Article
pubs.acs.org/JACS

Unequal Partnership: Asymmetric Roles of Polymeric Donor and Fullerene Acceptor in Generating Free Charge

Brett M. Savoie,*[,†] Akshay Rao,*[,‡] Artem A. Bakulin,[§] Simon Gelinas,[‡] Bijan Movaghar,[†] Richard H. Friend,[‡] Tobin J. Marks,*[,†] and Mark A. Ratner*[,†]

[†]Department of Chemistry, Northwestern University, Evanston, Illinois 20208, United States
[‡]Cavendish Laboratory, University of Cambridge, Cambridge CB3 0HE, United Kingdom
[§]FOM Institute AMOLF, 1098 XG Amsterdam, The Netherlands

Supporting Information

ABSTRACT: Natural photosynthetic complexes accomplish the rapid conversion of photoexcitations into spatially separated electrons and holes through precise hierarchical ordering of chromophores and redox centers. In contrast, organic photovoltaic (OPV) cells are poorly ordered, utilize only two different chemical potentials, and the same materials that absorb light must also transport charge; yet, some OPV blends achieve near-perfect quantum efficiency. Here we perform electronic structure calculations on large clusters of functionalized fullerenes of different size and ordering, predicting several features of the charge generation process, outside the framework of conventional theories but clearly observed in ultrafast electro-optical experiments described herein. We show that it is the resonant coupling of photogenerated singlet excitons to a high-energy manifold of fullerene electronic states that enables efficient charge generation, bypassing localized charge-transfer states. In contrast to conventional views, our findings suggest that fullerene cluster size, concentration, and dimensionality control charge generation efficiency, independent of exciton delocalization.

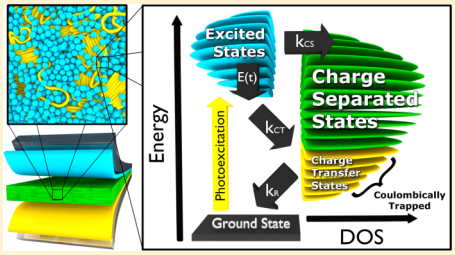

INTRODUCTION

In OPVs, charge generation occurs at the heterojunction between a donor (D) and an acceptor (A) semiconductor (Figure 1a). Individual photoexcitation of either component leads to the formation of singlet excitons, which decay within ns.[1,2] However, when these components are mixed to form a bulk-heterojunction blend, electron transfer (ET) occurs with high efficiency,[1] leading to charge-separated (CS) states (Figure 1c). In some materials systems, remarkably, all of the CS states can be collected as electrical current.[3,4] In other systems, a large fraction (or all) of the CS states is short-lived and recombines on a similar time scale to the singlet excitons.[5−9] In the latter, the common interpretation is that while charge transfer (CT) between the components occurs, the carriers fail to escape from the heterojunction.[6,10,11] These uncollectable, short-lived CS states are typically subclassified as Coulombically trapped CT states,[12] and their occurrence has been empirically connected with poor morphology[10,13] (Figure 1a) and/or nonfullerene acceptors.[5,8,9] Because a mechanistic understanding of the charge generation process is still lacking, the distinction between CS and CT states remains nonrigorous, and until now it has been unclear if CT states act as charge precursors or exclusively as loss channels during charge generation.[14] Similarly, while ample experimental evidence suggests a connection between morphology and charge generation,[13,15] no framework exists for evaluating what defines beneficial morphology or its effect on the charge generation process.

Extensions of Onsager theory[16−18] have been frequently applied to model OPV charge yield,[13] wherein charge generation occurs from a bound CT precursor by a thermally activated and electric field-assisted process. Notably, the ET event and heterojunction electronic structure are entirely absent from the Onsager description, which concerns the separation of a bound state and not its creation. While the Onsager mechanism may play some role at later times, its neglect of the ET event and assumption of thermal equilibrium render it incompatible with the consistently observed time scale of <100 fs[5,6,10] as well as the electric field (reported here) and temperature-independent[19,20] nature of charge generation (Figure 3). On this time scale, the dynamics of charge generation and CT cannot be separated, and thermally assisted generation is too slow to explain the experimental rates.[21]

Attempts to connect OPV charge generation rates with a Marcus process have also been unsuccessful.[22,23] Marcus theory and its extensions weight a Fermi's golden rule (FGR) electronic transition rate by the thermal equilibrium probability that the system is in the necessary transition state.[24] Notably, both central Marcus assumptions—thermal equilibrium and the transition-state definition in terms of environmental reorganization—are invalid for processes competitive with relaxation. In condensed media, it is also necessary to consider the

Received: December 2, 2013
Published: January 24, 2014

   dx.doi.org/10.1021/ja411859m | J. Am. Chem. Soc. 2014, 136, 2876−2884

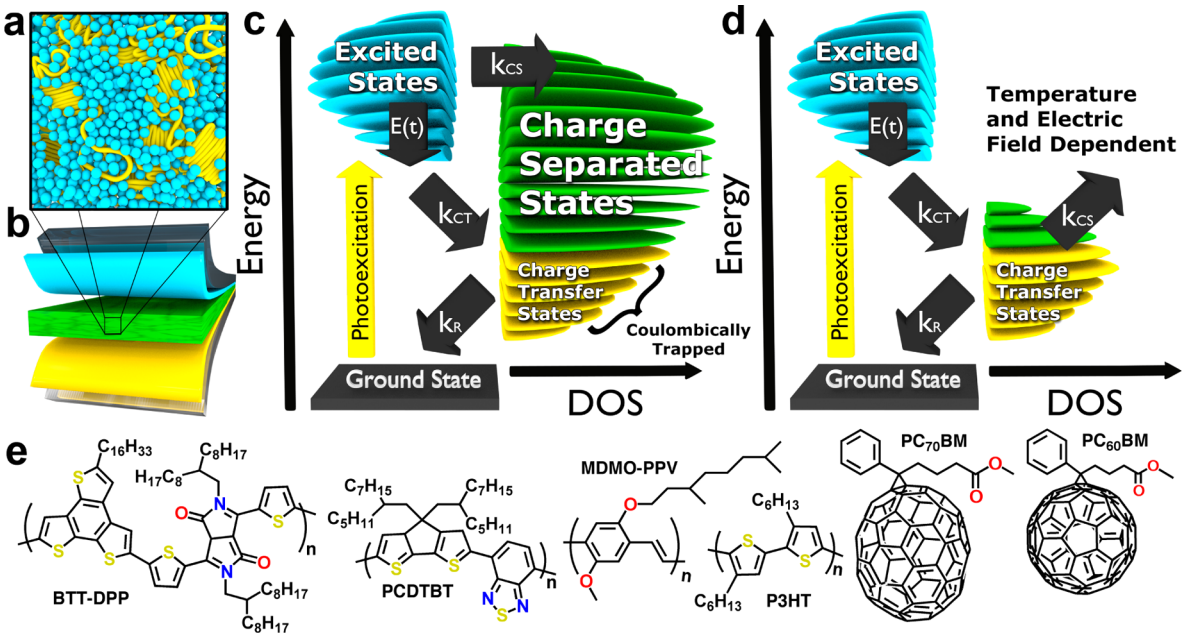

Figure 1. Fundamental charge generation processes, morphology, and device configuration in bulk-heterojunction organic photovoltaics. (a) Schematic depiction of the currently accepted bulk heterojunction microstructure with $PC_{60}BM$ acceptors (blue spheres) and polymer donors (gold strands) present with varying degrees of order and mixing. (b) Typical device configuration with the active layer (green) sandwiched between metallic and transparent electrodes. Interfacial layers (blue and gold) are chosen for selective extraction of electrons or holes. The states relevant to charge generation in (c) polymer:fullerene blends and (d) typical nonfullerene acceptor blends. Excited states (blue) predominantly occur in the donor phase with time-dependent localization and thermalization. In each case, the DOS accessible at the donor−acceptor heterojunction is depicted. In blends of fullerene (c), isoelectronic states resonant with the donor exciton facilitate charge generation directly. In nonfullerene blends (d), there is minimal accessibility to isoenergetic CS states, except through long-range tunneling or a Coulombically trapped intermediate. In each case, low-energy states are localized near the heterojunction and stabilized by the electron−hole Coulombic interaction. k_{CS} refers to the rate of CT to unbound separated states (CS), k_{CT} is the rate of CT to the low-energy Coulombically bound states (CT), and k_R is the rate of recombination. (e) Depicts the donors and acceptors used in this study.

availability of many states (Figure 1c), rather than the single transition typical of the Marcus picture (Figure 1d). In high-efficiency polymer:fullerene blends, the observed charge separation rates (k_{CS}) are invariably much faster (Figure 3c) than Marcus rates calculated between individual molecules.[23] Indeed, consistent experimental time scales for ET (<100 fs) strongly suggest a coherent, phase and energy conserving, electronic process, minimally influenced by nuclear reorganization. Thus, many fundamental observations of the charge generation process such as (i) the ultrafast time scale,[6,10] (ii) the temperature[11,19] and (iii) electric field independence of the initial charge yield, (iv) the unique free energy dependence of the charge yield,[11] and (v) the mechanistic differences in charge generation between polymer:polymer and polymer:fullerene blends[5,8,9] are not captured within the Marcus−Onsager framework.

Although fullerene acceptors are used in virtually all high performing OPVs, surprisingly, mechanistic explanations for efficient charge generation have focused mostly on the role of the donor component. Besides its ubiquitous use in devices, there are also several well-documented empirical observations that suggest the fullerene, and especially its aggregates, play a privileged role in the generation process. For instance, large increases in photocurrent[15] and carrier lifetime[6] occur when fullerene aggregates are formed[25,26] following annealing of P3HT:$PC_{60}BM$ blends. Several studies also show that intercalating systems, which disperse fullerene in stoichiometric proportions between polymer side chains, exhibit inefficient photocurrent production and reduced carrier lifetimes until sufficient fullerene is added to produce pure domains.[27,28] Here we develop a new model for charge generation which self-consistently explains the above experimental results and provides insights for the design of future materials.

RESULTS

Electronic Structure of Fullerene Aggregates. To understand the dynamics of charge generation in the most efficient polymer:fullerene blends it is crucial to identify the states that mediate this process. Recent results[5,10,29] hint that delocalized states play a role in charge separation, however no investigation of the relationship between extended states in the fullerene component and charge generation has yet been undertaken. To tackle this problem we performed large-scale simulations of the electronic structure of $PC_{60}BM$ clusters of varying size, ordering, and distribution of proximate positive charges (Figure 2b). Typical OPV active layer thicknesses are 100−200 nm, meaning no more than a few hundred fullerenes or polymer repeat units lie on any straight path between electrodes. This length scale is too large for explicit electronic structure calculations and too disordered[30] for periodic approaches. Thus we employed a simple fragment method of calculation that has proven predictive for assessing the electronic structure of disordered organic semiconductors[31] and large molecules.[32] Here, a basis of the three lowest unoccupied $PC_{60}BM$ molecular orbitals (MOs) (ϕ_i) is employed to calculate the unoccupied states of large $PC_{60}BM$ aggregates. Notably, fullerene is characterized by 3-fold degenerate LUMOs. Functionalization generally breaks this degeneracy, but the three LUMOs are still low-lying enough to

dx.doi.org/10.1021/ja411859m | J. Am. Chem. Soc. 2014, 136, 2876−2884

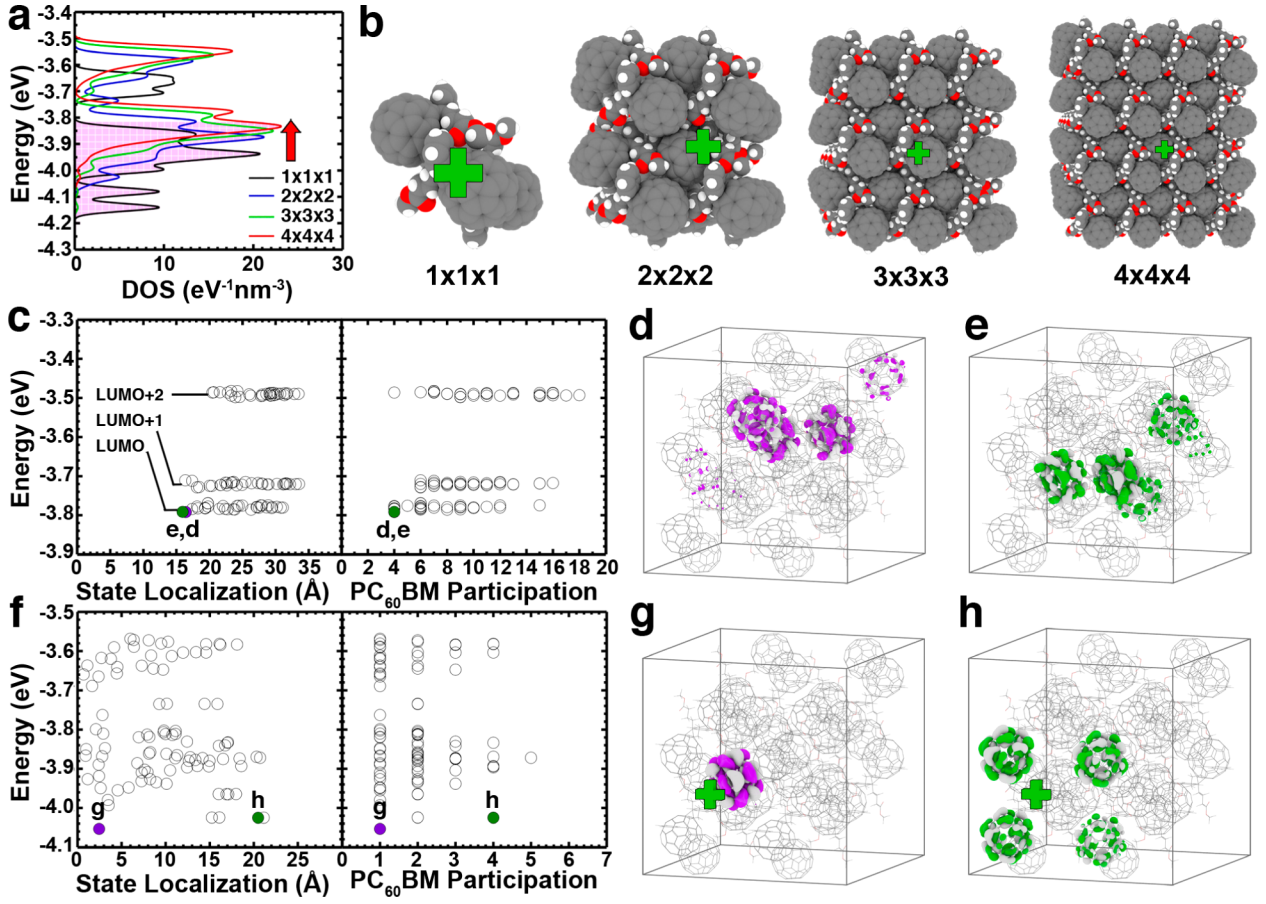

Figure 2. DOS calculations on PCBM crystallites of varying size. (a) The DOS of $PC_{60}BM$ clusters as a function of size, with a positive point charge placed 1 nm normal to the center of the fullerene front (001) face (this separation leads to ∼3 Å nearest-neighbor separation). Arrow indicates the reduced trap character with increasing cluster size. To make a direct comparison, each DOS has been normalized by the respective crystallite volume and states more than 26 meV (k_BT at room temperature) below the $PC_{60}BM$ LUMO level are designated in pink. Discrete eigenvalues were convoluted with a 5 meV Gaussian for the generation of the DOS and normalized by the respective cluster volume. (b) Geometries of the PC $_{60}$BM crystallites studied. A green "+" depicts the positive point charge. (c) Localization and $PC_{60}BM$ participation in 2 × 2 × 2 crystallite CS states in the absence of a positive point charge. Each dot corresponds to an eigenstate, while colored dots indicate states that are visualized in d and e. (f) Localization and $PC_{60}BM$ participation in 2 × 2 × 2 crystallite CS states, with a point charge included. Each dot corresponds to an eigenstate, while colored dots indicate states that are visualized in g and h. Note that the absolute energy of the CS states includes the ionization potential of the donor component. Since this varies from blend to blend, the energies are scaled to the ground state of $PC_{60}BM$.

participate in charge generation (Figure S7). The aggregate Hamiltonian, $\mathbf{H}_C$, has the form:

$$\mathbf{H}_C = \sum_{i,j}\left\{\left(\varepsilon_i + \sigma_i - \frac{q}{4\pi\varepsilon_0\varepsilon_r}\int dV\rho(\mathbf{r})\frac{1}{|\mathbf{r}_i - \mathbf{r}|}\right)|\phi_i\rangle\langle\phi_i| + V_{ij}|\phi_i\rangle\langle\phi_j|\right\} \quad (1)$$

where, ε_i is the orbital energy, σ_i the energetic site disorder, q the elementary charge, ε_0 and ε_r the vacuum and relative permittivity, respectively, $\mathbf{r}_i$ the centroid of the molecule containing ϕ_i, $\rho(r)$ an arbitrary charge distribution, and V_{ij} the electronic coupling between orbitals i and j. The CS states contributed by the $PC_{60}BM$ cluster were simulated by choosing $\rho(r)$ to represent a hole of varying delocalization outside the $PC_{60}BM$ cluster. This construction does not account for possible nuclear and electronic reorganizations (polaron formation) that might occur following the injection of a charge into the crystallite. The intention here is to characterize the electronic states in an unpertubed geometry that is consistent with the ultrafast time scale of the dynamics (a discussion of polaronic effects can be found in the SI). Thus, eq 1 represents the minimal construction capable of describing the electron transport states of the crystallite, how they are affected by disorder in energies and couplings, and the presence of a nearby positive charge distribution.

In initial simulations, $PC_{60}BM$ crystallites of varying sizes were generated by repeating the crystal unit cell reported by Rispens et al. (Figure 2b).[33] The crystallite unoccupied density of states (DOS) shows features typical of well-ordered systems, with modest band broadening with increasing size, and separated bands resulting from MO mixing (Figure S1). To characterize the spatial extent of individual states, both the localization (twice the standard deviation of the electron density) and number of $PC_{60}BM$ molecules participating in each state were assessed (see Methods). Figures 2c–e shows the localization and $PC_{60}BM$ participation in the 2 × 2 × 2 crystallite, along with direct visualization of several states. Most of the states are delocalized throughout the crystallites, with even the lowest energy states delocalized over several molecules.

While these results are informative, it is the CS state character in the presence of Coulombic stabilization that is most relevant to charge generation. Thus, a positive point

dx.doi.org/10.1021/ja411859m | J. Am. Chem. Soc. 2014, 136, 2876–2884

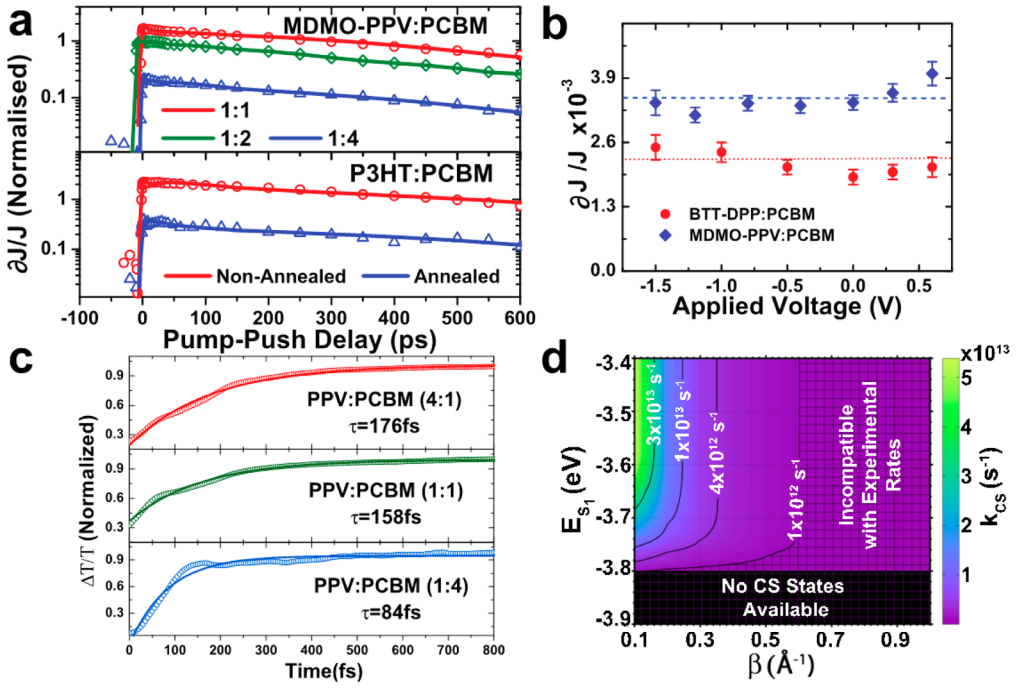

Figure 3. The rate of charge generation and the role of CT states in the indicated BHJ photovoltaic blends. (a) Pump−push−photocurrent data for (top panel) MDMO-PPV:$PC_{70}BM$ blends with varying $PC_{70}BM$ content and (bottom panel) annealed and nonannealed 1:1 blends of P3HT:PCBM. The amount of extra photocurrent ($\partial J/J$), and hence the yield of CT states, is found to be inversely proportional to fullerene domain size. Here $\partial J/J$ is normalized using the number of electron−hole pairs generated by the pump pulse and the absorption of the push pulse by these electron−hole pairs; see SI for details. (b) Pump−push−photocurrent data as a function of applied external bias. The fractional change in photocurrent, $\partial J/J$, is bias independent, indicating that the yield of CT states, and hence the initial charge generation process, is electric field independent. Here only the bias is varied on the same device keeping all other conditions equal, hence $\partial J/J$ can be used without further normalization (c) Rates of electron transfer, measured via the growth of the photoinduced absorption associated with hole-polarons, in MDMO-PPV:PCBM blends via transient absorption spectroscopy (see SI for details). Rates of electron transfer are found to be proportional to the fullerene domain size (d) Calculated rates of charge generation in 4 × 4 × 4 PCBM clusters as a function of excited-state energy and decay rate of the donor−acceptor couplings. For simplicity, the excited-state energy is reported as the single-particle electron energy (i.e., the LUMO level of the donor), while the absolute energy of the state depends on the ionization potential of the donor and the exciton binding energy. Each data point is averaged over 100 runs. Note that ultrafast charge separation rates imply larger couplings (>40 meV) and slower decays (β < 0.6 $Å^{-1}$) than typically considered in organic semiconductors.

charge was introduced 1 nm normal to the 001 face center of each crystallite (this displacement leads to ∼3 Å nearest-neighbor separation), and the resulting states calculated (Figure 2b). The effect on the DOS is immediately apparent in smaller crystallites (Figure 2a). While the DOS of the larger crystallites is much less perturbed and ample high-energy CS states are present, the majority of states in the small crystallites are Coulombically bound and lie well below the energy of a typical donor exciton. Energy alignment is critical for ultrafast CT, since energy must be conserved in the process. Thus, the availability of many high-energy states in the larger clusters constitutes a "hot" channel to dissociation that bypasses the trapped CT states, whereas the smaller clusters have relatively few high-energy unbound states to directly couple with the exciton. For comparison, we illustrate several 2 × 2 × 2 crystallite states in the presence of the point charge. The lowest eigenfunction (Figure 2g) shows the size contraction expected for a CT state: The orbital density is localized on a single $PC_{60}BM$ unit, and the energy of the states is ∼0.4 eV beneath the vacuum LUMO level. However, the next eigenfunction is already delocalized over several $PC_{60}BM$ molecules (Figure 2h), and throughout the remaining states the localization varies greatly.

The effect of hole delocalization (Figure S2) and various disorder types (Figure S3) on the CS state spatial extent were also investigated. Remarkably, the average state localization is mostly unaffected by rotational and translational disorder, due to the spherical topology and essentially isotropic electronic coupling of the $PC_{60}BM$ component (Figures S5−S6).[34] The data also suggest that while the dimensionality of hole delocalization (1-D vs 2-D) in the donor matters, the direction of the delocalization (parallel vs perpendicular to the crystallite face) has a greater effect.[12]

The unique robustness of the fullerene electronic structure to structural disorder seems critical for providing high state accessibility in the filamentous BHJ domains. In disordered OPV active layers, retaining at least one component that is robust to disorder is highly desirable and at least partially explains fullerene dominance as an effective acceptor and the success of minimally processed polymer:fullerene films. Indirect evidence for this can also be found by considering the extensive literature on alternative OPV acceptors. The mobilities of fullerene derivatives such as $PC_{60}BM$ are unremarkable relative to other high-performance n-type semiconductors,[35−37] and other molecular acceptors can be induced to form similar morphologies.[38−40] In each case, this indicates the general inability to explain the dominance of fullerene-based acceptors in terms of collection or morphological considerations alone and supports the view that the special contribution of the fullerene is to provide robust electrical connectivity even in

dx.doi.org/10.1021/ja411859m | J. Am. Chem. Soc. 2014, 136, 2876−2884

disordered BHJ architectures. Conversely, this is also in keeping with the observation that the relative advantage of fullerene-based acceptors vanishes in bilayer device architectures,[41,42] which seems to be general despite inherent problems in comparing bilayer devices across studies.[43,44] In spacious planar heterojunctions, even nonspherical acceptors provide sufficient CS state accessibility for efficient generation and collection, albeit only for those photoexcitations formed within the diffusion length of the heterojunction.

The Effect of Fullerene Aggregates on Dynamics. The present calculations suggest that aggregates of the fullerene component contribute the important resonant states, relevant for charge separation, due to the several low-lying accepting orbitals and ability to form 3-D networks, even in the presence of disorder (Figure S3).[31,33,34] In contrast, bulky insulating polymer substituents typically inhibit extended state formation in three dimensions.[30,45] Experimentally this should be reflected by an asymmetry in the charge generation dynamics with the D:A ratio. At high polymer-to-fullerene ratios, CS states energetically resonant and coupled with the exciton should be rare, and CT state characteristics will dominate the dynamics (Figure 1d). At high fullerene-to-polymer ratio, resonant CS states should be abundant, and CT states should play a minimal role (Figure 1c).

To test this idea, we performed ultrafast pump–push–photocurrent (PPC) experiments[5,7] on working OPV devices where $PC_{70}BM$ cluster formation was controlled. Here a visible pump pulse creates a population of singlet excitons that undergo ET at the heterojunction, forming both unbound CS states and trapped CT excitons. The latter can then be re-excited to higher electronic states via an IR push pulse, allowing them to dissociate and generate current. This extra photocurrent is then detected. Thus, the carrier fraction lost to CT states that could otherwise be collected as photocurrent can be assessed (see Methods). Fullerene cluster formation was controlled by studying MDMO-PPV films (Figure 1e), blended with $PC_{70}BM$ in 1:1, 1:2, and 1:4 donor:acceptor mass ratios. It is known that $PC_{70}BM$ efficiently intercalates into PPV and that pure $PC_{70}BM$ domains do not form in this system until a 1:2 ratio and are pronounced in a 1:4 ratio.[27] Annealed and unannealed films of the common donor P3HT blended with $PC_{70}BM$ in a 1:1 ratio were also studied. Here annealing facilitates $PC_{70}BM$ crystallite formation.[30,46]

Figure 3a shows the fractional change in photocurrent, $\partial J/J$, as a function of delay between pump and push. In both systems, $\partial J/J$, and hence the carrier fraction lost to the CT channel, is inversely related to the presence of pure $PC_{70}BM$ domains. The CT states also form on a similar or later time scale (<300 fs, determined by the onset of push response) to the CS states (Figure 3c), suggesting direct branching between the $[S_1] \rightarrow [CT]$ and $[S_1] \rightarrow [CS]$ channels and ruling out the [CT] state as a free charge precursor.[6,14] These observations, consistent across different donor polymers, support our suggestion that resonant states in the fullerene phase provide the channel for direct dissociation that bypasses the CT state.

The mechanism described here depends on the appropriate energy alignment between the excitonic and CS states at the heterojunction. This alignment should be unaffected by typical electric fields in the device and so predicts that the charge generation dynamics should be independent of electric field at early times. On the other hand, if dissociation proceeds through a CT precursor, separation should exhibit a field dependence associated with detrapping,[12,16,17] and the magnitude of the push response should be attenuated by the applied field. To test this possibility we performed PPC measurements as a function of applied external bias for MDMO-PPV:$PC_{70}BM$ and BTT-DPP:$PC_{70}BM$ devices (Figure 1d; see Methods). As shown in Figure 3b, $\partial J/J$, and hence the yield of trapped CT states, is found to be independent of the applied bias, indicating that the generation of free CS states in polymer:fullerene blends does not proceed through a trapped intermediate. Full transients are provided in the SI.

Taken together, the results on the effects of blend ratio, annealing, and electric field strongly suggest that a direct route, contributed by the fullerene component and bypassing the low-energy CT states (Figure 1c), is responsible for efficient photocurrent generation in polymer:fullerene systems. However, the likelihood of an excitation following this channel is determined by the specific couplings between the excitation and the unbound CS states (i.e., $V_{S_1,CS} = \langle \Psi_{S_1} | \mathbf{H}_C | \Psi_{CS} \rangle$), and the rate of competitive transfer to a localized CT state. To assess these couplings, an excitation coupled to the individual acceptors was included in eq 1, and the $V_{S_1,CS}$ couplings extracted during the Hamiltonian diagonalization procedure (see Methods). In the limit of minimal reorganization, k_{CS} can be calculated using Fermi's golden rule:

$$k_{CS} = \frac{2\pi}{\hbar} \sum_{E_{CT} < E < E_{S_1}} \left| \langle \Psi_{S_1} | \mathbf{H}_C | \Psi(E) \rangle \right|^2 \rho_{CS}(E) \tag{2}$$

where conservation of energy requires that the summation includes states lower in energy than the initial excitation (E_{S_1}), and ρ_{CS} is the density of CS states at each transition. Only transfer to unbound states is included by setting the lower summation limit to the upper edge of the charge-transfer manifold (E_{CT}). In this phenomenological model, an exciton of energy E_{S_1} can transfer to any state less than or equal in energy, with a rate proportional to the state coupling and DOS. In this way, we assess the roles of both the excitation energy and the availability of unbound states in the fullerene component (Figure 2a) on ET.

Figure 3d shows k_{CS} calculated for the $4 \times 4 \times 4$ crystallite as a function of E_{S_1} and decay of the donor–acceptor couplings ($\propto e^{-\beta(R-R_0)}$), which controls the long-range ET probability. Analogous calculations for smaller crystallites, which yield lower values of k_{CS}, are shown in Figure S8. We immediately note that reproducing experimental rates requires a combination of large couplings and slow decay of the coupling elements (i.e., permitting long-range transfer).[29] This is remarkable since eq 2 represents the upper limit of the transfer rate as Franck–Condon factors have implicitly been set to unity.[47] These results are compared with the experimental k_{CS} in Figure 3c, measured by monitoring the rise of the photoinduced absorption (PIA) of hole-polarons on MDMO-PPV:$PC_{60}BM$ using ultrafast transient absorption spectroscopy (see SI for details). Different blend ratios of MDMO-PPV:$PC_{60}BM$ were studied, and the rate of ET was found to be proportional to the weight fraction of $PC_{60}BM$, consistent with the decrease in k_{CS} with fullerene cluster size predicted by the model.

These results also show that the excited-state energy and fullerene crystallite size are the primary determinants of k_{CS}. This implies that the ΔG_{CS} dependence of charge yield is a property of the fullerene electronic structure and aggregation,[46,48] rather than the result of a Marcus-type ET to low-energy CT states. Indeed, the failure to observe Marcus

inverted behavior in any ultrafast study of polymer:fullerene blends to date[5,6,10,19] is explained by the availability of a direct high-energy channel bypassing the CT state and is predicted by our model. Inverted behavior should only be observable in systems with no isoenergetic CS states coupled to the exciton (e.g., molecular dispersions of fullerenes in polymers,[22] or systems with exceptionally high-energy excitations occurring above the broad CS excited-state band. Such systems are generally not considered useful for OPVs anyway because of poor spectral overlap with the solar spectrum and/or low device voltages). Additionally, the mechanism of direct $S_1 \rightarrow$ CS transfer clarifies the empirical observation that greater ΔG_{CS} often leads to enhanced charge generation.[11,49] Increasing either E_{S_1} or the crystallite size makes more CS states accessible for charge generation and offers the possibility of long-range separation,[29] while slower rates of ET are predicted and observed for smaller fullerene clusters with restricted access to CS states.

The concept of state accessibility also has critical importance for evaluating the entropic contribution to ΔG_{CS}. While increasing the excited-state energy obviously increases the enthalpic contribution to the free energy, it also potentially increases the entropic contribution by expanding the number of accessible states. The full expression for the system entropy is $S = k_B \sum_i^{\Omega} p_i \ln(p_i)$,where the summation, i, runs over all CS microstates (Ω), and p_i is the accessibility of each state. The standard approximation, $p_i = \Omega^{-1}$, which considers each state equally accessible, is clearly inappropriate for nonequilibrium processes. Using the present calculations on $PC_{60}BM$ aggregates, we can improve the estimate for the number of accessible states as a function of the exciton energy, by only including states less than or equal in energy to the initial excitation. In this way, the entropic dependence on the energy of the initial state is estimated by discarding energetically uphill states that are likely inaccessible on the time scale of charge generation. For each value of E_{S_1} the number of CS microstates was calculated and used to assess the upper limit of the entropic contribution to ΔG_{CS} as a function of aggregate size (Figure 4). The results show that both larger clusters and higher excitations entropically favor charge separation. Also, for fullerene derivatives like $PC_{60}BM$, both the total entropic contribution and its energy dependence are accentuated since each molecule contributes three states that are energetically relevant to the generation process. Thus, the entropic trends reinforce the promising electronic structure characteristics of fullerene clusters highlighted in the previous section. In our view, reports of the temperature independence[19,20] of the charge yield strongly suggest that the current generation of materials systems are kinetically, rather than thermodynamically, limited and imply that the entropic contribution plays a secondary role. However, utilizing the larger state accessibility of 3-D materials with high state degeneracy represents an exciting prospect for designing efficient low ΔH_{CS} systems.

We note that several studies of charge generation have highlighted the role of the 'mixed phase' where polymer and fullerene are intimately mixed. In agreement with the results presented above, it has been suggested that poor fullerene connectivity at the heterojunction[50,51] and phase impurities[27,28,52] can lead to suppressed photocurrents. In the model presented here, such failures are simply specific instances of the limited accessibility to CS states in the absence of pure fullerene domains. In contrast, structural studies capable of distinguishing between pure and mixed phases have shown that in high-performing blends, pure domains of fullerene around 4 nm large are formed.[53] It is precisely these length scales considered in the simulations above. Thus our results agree with the known morphological properties of efficient OPVs and provide a molecular level understanding of why these morphologies are optimal.

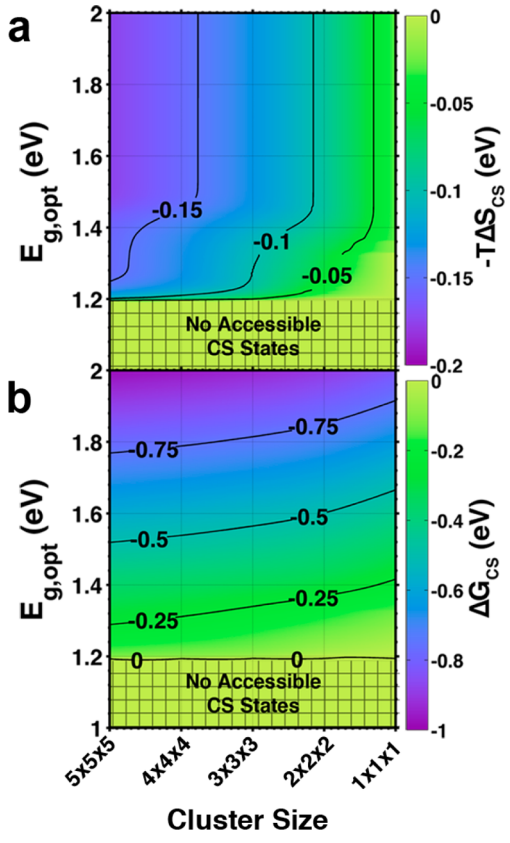

Figure 4. The effect of crystallite size on the thermodynamics of charge generation. The effect of cluster size and excitation energy on the entropy and free energy of charge generation. The free energy is calculated as $\Delta G_{CS} = E_{CT} - E_{g,opt} - T\Delta S$, where E_{CT} is the lowest unbound state (i.e., the upper edge of the CT state manifold). Here, E_{CT} is calculated as $IP_D + E_{LUMO} - k_B T$. Since IP_D varies from material to material, we consider a constant typical value of 5 eV and $T = 300$ K. Grid intersections correspond the explicitly calculated data points.

Role of Exciton Delocalization. In contrast to the view presented here, delocalization of the initial photoexcitation has been invoked to explain both the time scale of exciton quenching and the efficiency of dissociation.[10,54−56] While exciton delocalization provides a plausible mechanism for ultrafast exciton quenching, there is only indirect experimental evidence for the phenomenon, and it is unclear if delocalization is at all necessary for efficient charge generation. Indeed, several studies have found that charge generation following exciton diffusion is as efficient as early time charge generation from a presumably delocalized exciton.[6,54] Critically, if exciton delocalization in the donor were the primary determinant of charge generation efficiency, then geminate losses should be correspondingly independent of the acceptor used in the device. However, the opposite effect is widely observed experimentally,[7−9] as also evidenced by the ubiquitous use of fullerene derivatives in efficient devices (see SI for further discussion).

dx.doi.org/10.1021/ja411859m | J. Am. Chem. Soc. 2014, 136, 2876−2884

Subgap Excitation of Blends. Finally, the question of subgap excitation in polymer:fullerene blends is addressed. Numerous studies,[57−59] including our own,[5] have demonstrated that it is possible to excite such systems directly from the ground state to CT state manifold. It has been argued that charge generation from such 'cold' states suggests that the lowest-lying CT states can efficiently be dissociated. However, it is important to keep in mind the nature of the electronic states that can be generated via direct excitation from the ground state. The lowest-lying CT states are those that have undergone vibrational relaxation and polaron formation. Once the charge is placed on the polymer, this polaron formation proceeds extremely rapidly, in <100 fs.[5,60] However, these vibrationally relaxed states cannot be directly excited from the ground state, by definition, since the charges that give rise to them are not present on the polymer. The large charge distribution associated with CT transitions—a full charge moved, at a minimum, several Ångstroms—also renders the polaronic stabilization quite substantial, with both experimental and computational estimates placing it at ∼0.2−0.4 eV.[23,61] Thus, subgap excitation in OPV blends generates higher energy CT states, which can then relax further via polaron formation. But this means that the initially formed states can have sufficient energy that they are resonant with CS states (see Figure 1c), thereby allowing charges to directly escape from the heterojunction. Thus, in the presence of aggregated fullerene domains, subgap excitation can allow efficient charge generation, just as above gap excitation does, although further experiments using complementary techniques are required to quantify the relative efficiency of the two processes.

■ CONCLUSIONS

The mechanism of resonant ET suggested here, due to a high density of fullerene CS states energetically aligned with the donor exciton at the heterojunction, offers a new framework to understand efficient charge separation in organic semiconductor-based photovoltaics. This framework resolves several outstanding problems in the field, including the absence of Marcus inverted behavior in ultrafast studies[5,6,10,19] and the success of fullerene based acceptors in achieving high quantum efficiency of charge generation.[3,4] Furthermore, this mechanism comports with existing ultrafast spectroscopic characterizations of charge generation in polymer:fullerene blends. In particular, it is consistent with the: (i) ultrafast time scale, (ii) the direct [CT]:[CS] branching ratio, and (iii) electric field independence measured here. The mechanism is also consistent with the (iv) temperature independence measured by several groups[19,20] and (v) provides a quantifiable mechanism for the ΔG_{CS} dependence of charge generation.[11,49] Finally, this mechanism suggests that a crucial difference between polymer:fullerene and polymer:polymer OPVs lies in the direct electronic channel to dissociation provided by accessible high-energy fullerene CS states.[5] These findings underscore the importance of moving beyond single molecule ground-state descriptors in designing OPV materials. While it has long been considered advantageous to tune morphology for better "ordering", "crystallinity", and "domain size",[27,46] the connection between cluster size, localization, and the fractional availability of CS states demonstrated here provides the first direct connection between morphology and states that facilitate charge generation. Remarkably, we find that the charge generation features are largely determined by the morphology of the fullerene component, resulting in consistent features across the donor polymers studied here.

■ METHODS

Electronic Structure Calculations. Electronic structure evaluation of $PC_{60}BM$ and $PC_{70}BM$ single molecules was carried out with the Amsterdam Density Functional (ADF) Theory Package.[62,63] Reported energy levels are for geometry-optimized molecules utilizing augmented double-ζ, polarized basis sets with the B3LYP functional and Grimme's dispersion correction[64] (B3LYP-D3/ADZP). The pairwise electronic coupling integrals between molecules were calculated as $V_{ij} = \langle \phi_i | H | \phi_j \rangle$,where ϕ_i and ϕ_j are unoccupied orbitals on different $PC_{60}BM$ molecules.

Calculating the CS and CT States of Each Crystallite. Crystallite geometries were formed by repeating the unit cell reported by Rispens et al. for $PC_{60}BM$ crystallized from *o*-DCB.[33] For calculations including Coulomb interaction, the positive charge distribution was placed along the 001 face of the crystallite. The face was defined by the centroids of the $PC_{60}BM$ molecules in the 001 plane. A 1 nm separation from this face leads to ∼3 Å nearest-neighbor separation considered reasonable for organic materials. After assembling the Hamiltonian (eq 1), the crystallite states were obtained by solving the eigenproblem:

$$\mathbf{H}_C = \mathbf{U}\mathbf{D}\mathbf{U}^{-1} \tag{3}$$

where the matrix $\mathbf{U}$ holds the eigenfunctions of $\mathbf{H}_C$ in terms of $PC_{60}BM$ MO basis coefficients, and $\mathbf{D}$ holds the eigenvalues of $\mathbf{H}_C$ along its diagonal. The localization and participation ratio are standard characterization metrics for assessing the spatial dimensions of a wave function (see ref 31 for an example).

CT Rate Calculation. For evaluation of eq 2 a donor excited state of variable energy (E_{S_1}) was included in the Hamiltonian (eq 1). An exponential decay of the excited state with the individual acceptors (V_{DA}) was assumed $V_{DA}(R) = V_0 e^{-\beta(R-R_0)}$ with V_0 = 40 meV and R_0 = 1 nm. The Coulombic influence of the excitation on the cluster was assumed to be as a positive point charge. The data in Figure 3d were calculated in steps of 0.1 $Å^{-1}$ for the parameter β. Each data point is averaged over 100 geometries, where the excitation was placed at a random position in the plane normally displaced 1 nm and parallel to the 001 crystallite face. The crystallite eigenfunctions were obtained as described above. After obtaining the transformation matrix $\mathbf{U}$ (i.e., the eigenfunctions of the crystallite subsubsystem), we extend both $\mathbf{U}$ and $\mathbf{H}_C$ to include the excitation. $\mathbf{H}_C$ includes an entry for the excited-state energy along the diagonal at $H_{i,i}$, and the couplings of the excited state with the individual acceptors are included along row and column *i*. The transformation matrix $\mathbf{U}$ includes entries $U_{i,x} = U_{x,i} = \delta_{x,i}$ to accommodate the excitation. The couplings between the donor excited state and the crystallite eigenstates are obtained as the off-diagonal matrix elements in $\mathbf{D}$ (where $\mathbf{D} = \mathbf{U}^{-1}\mathbf{H}_C\mathbf{U}$). The rate, k_{CS}, is obtained by integrating (eq 2) over all states lower in energy than E_{S_1} and above the CT manifold edge. The upper edge of the CT manifold, E_{CT}, is defined as the vacuum LUMO level of $PC_{60}BM$ minus the ambient thermal energy (26 meV).

Pump−Push Photocurrent Experiments. Recently the technique of pump−push photocurrent spectroscopy has been developed and shown to enable the direct probing of trapped CT states.[5] In this technique an ultrafast pump pulse generates singlet states in either donor or acceptor material. Following singlet dissociation via ultrafast CT at the heterojunction a certain fraction of the CS states become trapped as CT states, which relax electronically and vibrationally (polaron formation) to the lowest-lying CT level. These CT states are then re-excited by an ultrafast IR-push pulse tuned to a wavelength corresponding to the P1 transition[2] of the hole-polaron on the polymer. This promotes the relaxed CT state to a higher lying electronically level, allowing them another chance to separate into free charges, giving rise to an extra photocurrent that is detected in the experiment. For measurements presented here pump pulses were generated using the output of a home-built noncollinear optical

parametric amplifier (OPA) and push pulses via a commercial OPA (TOPAS, Light Conversion), both seeded by the output of a Ti:sapphire amplifier (Spectra Physics, Solstice, 90 fs, 1kHz). Pump and push pulses were focused on the same spot of a working device. Unless stated otherwise the device was held at short circuit conditions. A delay between pump and push pulse is generated via a mechanical delay stage (Thorlabs). Current induced by the pump pulse (1 kHz) was detected using a lock in amplifier (Stanford Instruments) working in current mode. The push pulse was mechanically chopped at 370 Hz and the extra photocurrent generated, ∂J, detected using another lock in amplifier (Stanford Instruments). The fractional change in photocurrent, $\partial J/J$, can then be calculated. When the push pulse arrives before the pump pulse (negative times) no extra photocurrent is generated, as there are no electron−holes pairs within the device. After time zero the push pulse arrives after the pump pulse and induces an extra photocurrent. For data shown in Figure 3a $\partial J/J$ is normalized by the number of electron−hole pairs generated by the pump pulse and the number of IR-push photons absorbed by each such pair (always <1). This normalization allows for a comparison of $\partial J/J$ between different devices and materials. For data shown in Figure 3b this normalization is not needed as data are for a single device with only a variation of bias. Full details of the pump−push pulse wavelengths and fluence as well as J and ∂J can be found in the SI.

Materials. P3HT was obtained from Merck, MDMO-PPV from Sigma Aldrich and $PC_{70}BM$ from Nano-C. BTT-DPP was synthesized as described previously.[65]

Device Fabrication. Devices consisted of ITO/PEDOT:PSS/active-layer/Al. Blends of PPV:$PC_{71}BM$ (1:1, 1:2 or 1:4 in chlorobenzene), P3HT:$PC_{71}BM$ (1:1 in dichlorobenzene), and BTT-DPP:PCBM (1:3 in dichlorobenzene) were prepared in a glovebox. PEDOT:PSS was spun on the cleaned and plasma-treated ITO substrates and dried (150 C, 30 min) before being transferred to a nitrogen glovebox where the active layer was spin coated, followed by deposition of Al electrodes. For BTT-DPP:PC70BM 1 nm of LiF was deposited before Al.[11] All samples were encapsulated before testing.

■ ASSOCIATED CONTENT

Ⓢ Supporting Information

Orientational dependence of $PC_{60}BM$ electronic coupling, effect of energetic disorder on crystallite electronic structure, full spectroscopic transients, and additional discussion of some results. This material is available free of charge via the Internet at http://pubs.acs.org.

■ AUTHOR INFORMATION

Corresponding Authors

brettsavoie@u.northwestern.edu
ar525@cam.ac.uk
t-marks@northwestern.edu
ratner@northwestern.edu

Notes

The authors declare no competing financial interest.

■ ACKNOWLEDGMENTS

We thank S. Dimitrov, J. Durrant, and I. McCulloch for the BTT-DPP:$PC_{70}BM$. B.M.S. thanks N. E. Jackson and K. L. Kohlstedt for useful discussions of the results. B.M.S. was supported as part of the ANSER Center, an Energy Frontier Research Center funded by the U.S. Department of Energy, Office of Science, Office of Basic Energy Sciences, under award no. DE-SC0001059. B.M.S. also thanks the Northwestern Materials Science and Engineering Center (NSF Grant DMR-1121262) for a graduate fellowship in excitonics. A.R. thanks Corpus Christi College, Cambridge, for a Research Fellowship. A.A.B. acknowledges a VENI grant from The Netherlands Organization for Scientific Research (NWO). The work in Cambridge was supported by the EPSRC. M.A.R. thanks the U.S.-Israel Binational Science Foundation (grant 2011509).

■ REFERENCES

(1) Sariciftci, N. S.; Smilowitz, L.; Heeger, A. J.; Wudl, F. *Science* **1992**, *258*, 1474.
(2) Österbacka, R.; An, C. P.; Jiang, X. M.; Vardeny, Z. V. *Science* **2000**, *287*, 839.
(3) Schilinsky, P.; Waldauf, C.; Brabec, C. J. *Appl. Phys. Lett.* **2002**, *81*, 3885.
(4) Park, S. H.; Roy, A.; Beaupré, S.; Cho, S.; Coates, N.; Moon, J. S.; Moses, D.; Leclerc, M.; Lee, K.; Heeger, A. J. *Nat. Photonics* **2009**, *3*, 297.
(5) Bakulin, A. A.; Rao, A.; Pavelyev, V. G.; Van Loosdrecht, P. H. M.; Pshenichnikov, M. S.; Niedzialek, D.; Cornil, J.; Beljonne, D.; Friend, R. H. *Science* **2012**, *335*, 1340.
(6) Howard, I. A.; Mauer, R.; Meister, M.; Laquai, F. *J. Am. Chem. Soc.* **2010**, *132*, 14866.
(7) Muller, J.; Lupton, J.; Feldmann, J.; Lemmer, U.; Scharber, M.; Sariciftci, N.; Brabec, C.; Scherf, U. *Phys. Rev. B* **2005**, *72*, 195208.
(8) Hodgkiss, J. M.; Campbell, A. R.; Marsh, R.; Rao, A.; Albert-Seifried, S.; Friend, R. *Phys. Rev. Lett.* **2010**, *104*, 177701.
(9) McNeill, C. R.; Westenhoff, S.; Groves, C.; Friend, R. H.; Greenham, N. C. *J. Phys. Chem. C* **2007**, *111*, 19153.
(10) Grancini, G.; Maiuri, M.; Fazzi, D.; Petrozza, A.; Egelhaaf, H.-J.; Brida, D.; Cerullo, G.; Lanzani, G. *Nat. Mater.* **2012**, *12*, 29.
(11) Dimitrov, S. D.; Bakulin, A. A.; Nielsen, C. B.; Schroeder, B. C.; Du, J.; Bronstein, H.; McCulloch, I.; Friend, R.; Durrant, J. R. *J. Am. Chem. Soc.* **2012**, *134*, 18189.
(12) Deibel, C.; Strobel, T.; Dyakonov, V. *Adv. Mater.* **2010**, *22*, 4097.
(13) Veldman, D.; Ipek, O.; Meskers, S. C. J.; Sweelssen, J.; Koetse, M. M.; Veenstra, S. C.; Kroon, J. M.; van Bavel, S. S.; Loos, J.; Janssen, R. A. J. *J. Am. Chem. Soc.* **2008**, *130*, 7721.
(14) Jailaubekov, A. E.; Willard, A. P.; Tritsch, J. R.; Chan, W.-L.; Sai, N.; Gearba, R.; Kaake, L. G.; Williams, K. J.; Leung, K.; Rossky, P. J.; Zhu, X.-Y. *Nat. Mater.* **2013**, *12*, 66.
(15) Li, G.; Shrotriya, V.; Huang, J.; Yao, Y.; Moriarty, T.; Emery, K.; Yang, Y. *Nat. Mater.* **2005**, *4*, 864.
(16) Hilczer, M.; Tachiya, M. *J. Phys. Chem. C* **2010**, *114*, 6808.
(17) Braun, C. *J. Chem. Phys.* **1984**, *80*, 4157.
(18) Onsager, L. *Phys. Rev.* **1938**, *54*, 554.
(19) Pensack, R.; Asbury, J. *J. Am. Chem. Soc.* **2009**, *131*, 15986.
(20) Murthy, D.; Gao, M.; Vermeulen, M.; Siebbeles, L. D. A.; Savenije, T. J. *J. Phys. Chem. C* **2012**, *116*, 9214.
(21) Servaites, J. D.; Savoie, B. M.; Brink, J. B.; Marks, T.; Ratner, M. *Energy Environ. Sci.* **2012**, *5*, 8343.
(22) Coffey, D. C.; Larson, B. W.; Hains, A. W.; Whitaker, J. B.; Kopidakis, N.; Boltalina, O. V.; Strauss, S. H.; Rumbles, G. *J. Phys. Chem. C* **2012**, *116*, 8916.
(23) Liu, T.; Troisi, A. *J. Phys. Chem. C* **2011**, *115*, 2406.
(24) Marcus, R. A. *Rev. Mod. Phys.* **1993**, *65*, 599.
(25) Watts, B.; Belcher, W. J.; Thomsen, L.; Ade, H.; Dastoor, P. C. *Macromolecules* **2009**, *42*, 8392.
(26) Campoy-Quiles, M.; Ferenczi, T.; Agostinelli, T.; Etchegoin, P. G.; Kim, Y.; Anthopoulos, T. D.; Stavrinou, P. N.; Bradley, D. D. C.; Nelson, J. *Nat. Mater.* **2008**, *7*, 158.
(27) Mayer, A. C.; Toney, M. F.; Scully, S. R.; Rivnay, J.; Brabec, C. J.; Scharber, M.; Koppe, M.; Heeney, M.; Mcculloch, I.; Mcgehee, M. D. *Adv. Funct. Mater.* **2009**, *19*, 1173.
(28) Rance, W. L.; Ferguson, A. J.; McCarthy-Ward, T.; Heeney, M.; Ginley, D. S.; Olson, D. C.; Rumbles, G.; Kopidakis, N. *ACS Nano* **2011**, *5*, 5635.
(29) Caruso, D.; Troisi, A. *Proc. Natl. Acad. Sci. U.S.A.* **2012**, *109*, 13498.
(30) Rivnay, J.; Mannsfeld, S. C. B.; Miller, C. E.; Salleo, A.; Toney, M. F. *Chem. Rev.* **2012**, *10*, 5488.

(31) Cheung, D. L.; Troisi, A. *J. Phys. Chem. C* **2010**, *114*, 20479.
(32) Kitaura, K.; Ikeo, E.; Asada, T.; Nakano, T.; Uebayasi, M. *Chem. Phys. Lett.* **1999**, *313*, 701.
(33) Rispens, M. T.; Brabec, C.; Sariciftci, N.; Hummelen, J. *Chem. Commun.* **2003**, 2116.
(34) MacKenzie, R. C. I.; Frost, J. M.; Nelson, J. *J. Chem. Phys.* **2010**, *132*, 064904.
(35) Wöbkenberg, P. H.; Bradley, D. D. C.; Kronholm, D.; Hummelen, J. C.; Leeuw, D. M. d.; Cölle, M.; Anthopoulos, T. D. *Synth. Met.* **2008**, *158*, 468.
(36) Lenes, M.; Shelton, S.; Sieval, A.; Kronholm, D. F.; Hummelen, J. C.; Blom, P. W. M. *Adv. Funct. Mater.* **2009**, *19*, 3002.
(37) Anthony, J. E.; Facchetti, A.; Heeney, M.; Marder, S. R.; Zhan, X. *Adv. Mater.* **2010**, *22*, 3876.
(38) Sharenko, A.; Proctor, C. M.; Van Der Poll, T. S.; Henson, Z. B.; Nguyen, T.-Q.; Bazan, G. C. *Adv. Mater.* **2013**, *25*, 4403.
(39) Rajaram, S.; Shivanna, R.; Kandappa, S. K.; Narayan, K. S. *J. Phys. Chem. Lett.* **2012**, 1.
(40) Dittmer, J.; Marseglia, E.; Friend, R. *Adv. Mater.* **2000**, *12*, 1270.
(41) Halls, J.; Friend, R. H. *Synth. Met.* **1997**, *85*, 1307.
(42) Holcombe, T. W.; Norton, J. E.; Rivnay, J.; Woo, C. H.; Goris, L.; Piliego, C.; Griffini, G.; Sellinger, A.; Bredas, J.-L.; Salleo, A.; Frechet, J. M. J. *J. Am. Chem. Soc.* **2011**, *133*, 12106.
(43) Gevaerts, V. S.; Koster, L. J. A.; Wienk, M. M.; Janssen, R. A. J. *ACS Appl. Mater. Interfaces* **2011**, *3*, 3252.
(44) Markov, D.; Amsterdam, E.; Blom, P.; Sieval, A.; Hummelen, J. *J. Phys. Chem. A* **2005**, *109*, 5266.
(45) In this regard, vacuum deposited small molecules without solubilizing side-chains may offer an advantage.
(46) Jamieson, F. C.; Domingo, E. B.; Mccarthy-Ward, T.; Heeney, M.; Stingelin, N.; Durrant, J. R. *Chem. Sci.* **2012**, *3*, 485.
(47) Barbara, P.; Meyer, T. J.; Ratner, M. A. *J. Phys. Chem.* **1996**, *100*, 13148.
(48) Kwlatkowski, J. J.; Frost, J. M.; Nelson, J. *Nano Lett.* **2009**, *9*, 1085.
(49) Clarke, T. M.; Durrant, J. R. *Chem. Rev.* **2010**, *110*, 6736.
(50) Bartelt, J.; Beiley, Z.; Hoke, E. T.; Mateker, W. R.; Douglas, J. D.; Collins, B. A.; Tumbleston, J. R.; Graham, K. R.; Amassian, A.; Ade, H.; Frechet, J. M. J.; Toney, M. F.; McGehee, M. D. *Adv. Energy Mater.* **2013**, *3*, 364.
(51) Ma, W.; Tumbleston, J. R.; Wang, M.; Gann, E.; Huang, F.; Ade, H. *Adv. Energy Mater.* **2013**, *3*, 864.
(52) Chen, H.; Peet, J.; Hu, S.; Azoulay, J.; Bazan, G.; Dadmun, M. *Adv. Funct. Mater.* **2014**, *24*, 140.
(53) Collins, B. A.; Li, Z.; Tumbleston, J. R.; Gann, E.; Mcneill, C. R.; Ade, H. *Adv. Energy Mater.* **2012**, *3*, 65.
(54) Kaake, L. G.; Moses, D.; Heeger, A. J. *J. Phys. Chem. Lett.* **2013**, *4*, 2264.
(55) Moses, D.; Wang, J.; Heeger, A.; Kirova, N.; Brazovski, S. *Proc. Natl. Acad. Sci. U.S.A.* **2001**, *98*, 13496.
(56) Miranda, P.; Moses, D.; Heeger, A. *Phys. Rev. B* **2001**, *64*, 081201.
(57) Vandewal, K.; Albrecht, S.; Hoke, E. T.; Graham, K. R.; Widmer, J.; Douglas, J. D.; Schubert, M.; Mateker, W. R.; Bloking, J. T.; Burkhard, G. F.; Sellinger, A.; Fréchet, J. M. J.; Amassian, A.; Riede, M. K.; Mcgehee, M. D.; Neher, D.; Salleo, A. *Nat. Mater.* **2013**, *12*, 1.
(58) Lee, J.; Vandewal, K.; Yost, S. R.; Bahlke, M. E.; Goris, L.; Baldo, M. A.; Manca, J. V.; Van Voorhis, T. *J. Am. Chem. Soc.* **2010**, *132*, 11878.
(59) Drori, T.; Sheng, C. X.; Ndobe, A.; Singh, S.; Holt, J.; Vardeny, Z. V. *Phys. Rev. Lett.* **2008**, *101*, 037401.
(60) Clark, J.; Nelson, T.; Tretiak, S.; Cirmi, G.; Lanzani, G. *Nat. Phys.* **2012**, *8*, 225.
(61) Vandewal, K.; Tvingstedt, K.; Gadisa, A.; Inganas, O.; Manca, J. V. *Phys. Rev. B* **2010**, *81*, 125204.
(62) Fonseca Guerra, C.; Snijders, J. G.; te Velde, G.; Baerends, E. J. *Theor. Chem. Acc.* **1998**, *99*, 391.
(63) te Velde, G.; Bickelhaupt, F. M.; van Gisbergen, S. J. A.; Fonseca Guerra, C.; Baerends, E. J.; Snijders, J. G.; Ziegler, T. *J. Comput. Chem.* **2001**, *22*, 931.
(64) Grimme, S.; Antony, J.; Ehrlich, S.; Krieg, H. *J. Chem. Phys.* **2010**, *132*, 154104.
(65) Dimitrov, S.; Nielsen, C.; Shoaee, S.; Tuladhar, P. S.; Du, J.; McCulloch, I.; Durrant, J. R. *J. Phys. Chem. Lett.* **2012**, *3*, 140.